Key Points:
- Seasonal variations in organic matter inputs and temperature regulate oxygen consumption in intertidal beach aquifers
- Retention of fresh particulate organic matter in the sand body in summer leads to a highly reactive top layer in the beach infiltration zone
- Seasonal variations of organic carbon content in the fine fraction of the sediments indicate rapid organic matter turnover and low storage

Author Contributions:

Conceptualization: F. Auer, S. Ahmerkamp, M. Holtappels
Data curation: F. Auer, J. Cueto
Formal analysis: F. Auer, J. Cueto, C. Winter
Funding acquisition: C. Winter, M. Holtappels
Investigation: F. Auer, S. Ahmerkamp, J. Cueto, M. Holtappels
Methodology: F. Auer, S. Ahmerkamp, M. Holtappels
Project administration: M. Holtappels
Resources: M. Holtappels
Supervision: M. Holtappels
Visualization: F. Auer

Extensive Oxygen Consumption in the Intertidal Infiltration Zone of Beach Aquifers—The Impact of Seasonal Input, Filtration Efficiency, and Morphodynamics

F. Auer[1,2] , S. Ahmerkamp[3,4] , J. Cueto[5,6] , C. Winter[5] , and M. Holtappels[1]

[1]Alfred Wegener Institute Helmholtz Center for Polar and Marine Research, Bremerhaven, Germany, [2]Faculty of Geosciences, University of Bremen, Bremen, Germany, [3]Department of Biogeochemistry, Max-Planck-Institute for Marine Microbiology, Bremen, Germany, [4]Leibniz Institute for Baltic Sea Research, Rostock, Germany, [5]Institute of Geosciences, Christian-Albrechts-University Kiel, Kiel, Germany, [6]Department of Natural and Exact Sciences, Research Group in Natural and Exact Sciences—GICNEX, Universidad de la Costa, Barranquilla, Colombia

Abstract Seawater infiltration into the permeable sands of beach aquifers creates a high input of biogeochemical reactants driven by tides and waves. The upper sand layer acts as a filter, retaining particulate organic matter (POM), which is degraded by bacteria under predominantly oxic conditions. The seasonal variation of seawater POM and oxygen (O_2) entering the infiltration zone, combined with the POM filtration efficiency of the highly morphodynamic upper layer, determines the organic matter turnover and subsequent redox gradients along porewater flowpaths. We investigated these effects by quantifying the seasonal O_2 consumption rates directly from the incubations of sediments taken along a transect in the seawater infiltration zone at Spiekeroog Beach, Germany. We carried out a two-monthly year-long sampling campaign with high spatial resolution measurements down to 1 m depth. In summer, O_2 consumption rates of up to 106 μM hr^{-1} were found in the first decimeters with a significant decline over depth, indicating efficient retention of reactive POM in the surface layer. Seasonal variation in organic carbon of the sand's suspendable particulates indicates rapid turnover and little storage. In winter, rates decreased significantly to below 11 μM hr^{-1}. Integrated over the investigated oxic layer, the estimated carbon mineralization varies between 15 (winter) and 143 (summer) mmol C m^{-2} d^{-1} with a yearly average of 73 mmol C m^{-2} d^{-1}. The yearly CO_2 production of 35 kg per meter shoreline characterizes the beach as a high-throughout system with rapid OM remineralization in the retention layer, especially in summer, but with little OM storage.

Plain Language Summary On the coast, sandy beaches act as a filter for seawater. Seawater seeps into the sand, and organic particles such as algae remains are trapped between the sand grains. Bacteria live on the surface of the sand grains and use the oxygen dissolved in seawater to break down the organic material. We investigated how seasonal changes from spring to winter, and the particle filtration affects the oxygen consumption by bacteria. Our study found that oxygen consumption follows the availability of fresh algal material during the year and is greatest in summer, when temperatures are high and algal blooms are intense. This cycle determines when and where in the sediment bacteria are active and controls the breakdown of the organic algae material to carbon dioxide (CO_2). We found that overall bacteria in the beach sands degrade a high amount of organic matter compared to other sandy seabeds. Our findings therefore give valuable information on bacterial activity present in beach sands, which impacts the breakdown of organic material and determines the quality of the beach groundwater that ultimately flows back into the ocean. These processes impact the health of coastal ecosystems and have consequences for human activities, such as fisheries or recreation.

1. Introduction

Sandy beaches mark the highly dynamic land-ocean transition on more than 30% of the world's ice-free coastline (Luijendijk et al., 2018). These popular coastal landforms are highly dynamic sedimentary systems, driven mainly by the continuous interplay of tides and waves and the geological preconditions. In the beach subsurface, substances are transported to and recycled back from the ocean through advective porewater flow within the surficial sediments as part of the water cycle. The intertidal beach aquifer, which connects the inland aquifer to the open ocean, is considered a particularly reactive zone in this context (Anschutz et al., 2009; Moore, 1999; Wilson et al., 2024). This biogeochemical beach reactor plays an important role in coastal ecosystems, as it modulates material fluxes through subsurface biogeochemical reactions and is characterized by strong physical and chemical

Writing – original draft: F. Auer,
J. Cueto, M. Holtappels
Writing – review & editing: F. Auer,
S. Ahmerkamp, J. Cueto, C. Winter,
M. Holtappels

gradients (Beck et al., 2017; Charbonnier et al., 2022; Kim et al., 2017; Reckhardt et al., 2015). The transport patterns within the beach aquifer are formed by the interplay of tidal pumping, fresh groundwater discharge, and dense seawater circulation. Tidally driven transport typically shapes a seawater recirculation cell in the intertidal aquifer of the beach, known as the upper saline plume (USP, Figure 1c) (Robinson et al., 2006). At the beach face, seawater infiltration into the USP creates a high input of organic matter (OM) and electron acceptors such as oxygen (O_2). This supplies the sandy beach, that is, otherwise characterized by a low standing stock in organic carbon (OC) with fresh biogeochemical reactants and fuels the reactor's microbial activity (Ahrens et al., 2020; Anschutz et al., 2009; Huettel & Rusch, 2000; Kim et al., 2019).

Understanding the functioning of this coastal biogeochemical reactor requires a detailed and mechanistic knowledge of the governing processes and their dynamics. The supply of the reactants to the reactor through the seawater infiltration zone is regulated by the respective compound concentrations in the seawater and the tidally driven transport. In this zone, studies of porewater concentrations indicate that the biogeochemical processes are strongly influenced by seasonal fluctuations in seawater constituents and temperature (T) as a result of a strong benthic-pelagic coupling (Ahrens et al., 2020; Charbonnier et al., 2013; Cogswell & Heiss, 2021). Thus far, biogeochemical investigations of beach aquifers have mainly focused on sheltered beaches subjected to low to moderate wave and tidal forces (Massmann et al., 2023). Only a few studies have been conducted in high-energy settings, where strong waves and tides constantly reshape the beach morphology. Model results suggest the coupling of beach morphodynamics with the development of transient subsurface flow paths, forming a unique microbial habitat that differs from other more stable subsurface environments (Greskowiak et al., 2023; Massmann et al., 2023). These changing water flow paths assume additional variability in the supply of reactants for biogeochemical reactions in the subsurface (Waska et al., 2019), a complex interplay that has not yet been sufficiently researched.

In coastal and shelf waters, subtidal and intertidal sandy sediments play a key role in the turnover and cycling of nutrients and OC (Boudreau et al., 2001; Huettel et al., 2014; Rao et al., 2007). Their high permeability allows pore water advection, whereby a microbial community residing on sand grains lives on and modifies the introduced substances (Ahmerkamp et al., 2020; Probandt et al., 2018). In this way, they regulate the subsurface biogeochemistry and influence substance export to the coastal ocean through submarine groundwater discharge. The low stock of OC in these sandy sediments implies that heterotrophic bacterial processes are potentially limited by the availability of OM (Boudreau et al., 2001). The seawater infiltration zone marks the only boundary through which larger quantities of fresh OM can enter the reactor, thus regulating the biogeochemical turnover. In the shallow beach subsurface, results from porewater O_2 and nutrient concentration measurements led to the conclusion that aerobic respiration predominates the remineralization of OM (Charbonnier et al., 2013) and that this O_2 consumption is driven by seasonal variabilities in porewater T and the quality and quantity of supplied OM (Ahrens et al., 2020; Calvo-Martin et al., 2021). Additionally, sediment-entrapped particulate OM (POM) has been suggested to play a key role in the distribution of reaction patterns (Charbonnier et al., 2022; Kim et al., 2019, 2020). However, reaction rates of microbial OM turnover in the infiltration zone have rarely been measured directly and to our knowledge never at high spatial resolution over an entire year. However, such measurements provide valuable insights into subsurface OC remineralization and the reactivity of supplied OM, the main driver of biogeochemical turnover in beach aquifers and a key parameter for the regulation of subsurface redox conditions.

So far, rate measurements have not been linked to the combined impacts of seasonal OM availability, POM retention, and beach morphodynamics. Intertidal sands exposed to high energy conditions are characterized by high supply of oxidants and thus a substantial expansion of redox zones, allowing for extensive aerobic OM turnover (McLachlan & Turner, 1994). In the shallow subsurface of the seawater infiltration zone, the constant supply of reactants under advective flow promotes rapid turnover of OM under oxic conditions. Meanwhile, the transport of dissolved and particulate compounds within the sand body diverges, which suggests a spatially heterogeneous distribution of OM degradation rates. Based on these dynamics, we hypothesize that seasonal variations in OM availability significantly impact O_2 consumption rates in the upper infiltration zone. Specifically, we propose that increased rates during warmer months drive extensive OM turnover, whereas the retention of reactive POM enhances the spatial heterogeneity of decomposition rates. This seasonal shift is likely to have a significant impact on subsurface O_2 dynamics and subsequent OM mineralization pathways.
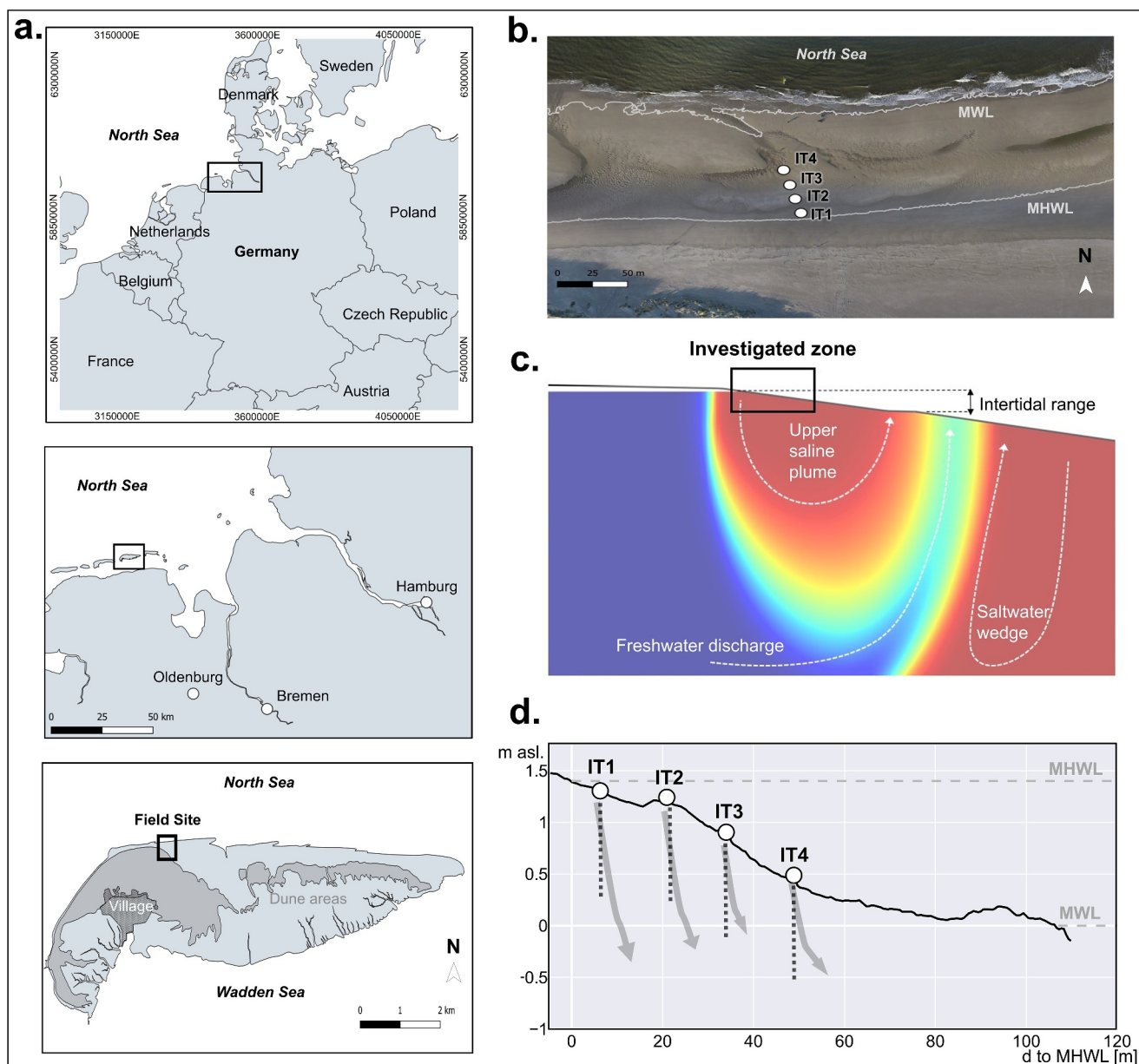
Figure 1. (a) Location of field site; (b) Infiltration zone transect on the beach (IT 1–4), drone photo, and locations from October 2022 between mean high water line (MHWL, 1.4 m asl) and mean water line (MWL, 0 m asl); (c) General flow patterns of saltwater (red) and freshwater (blue) in the subterranean estuary (Massmann et al., 2023; Robinson et al., 2006). (d) Details of investigated zone in the study, including beach topography (October 2022) and sampled depth (dotted black line). The arrows indicate the general advective porewater flow due to tidal pumping with arrow size corresponding to expected porewater velocities.

The objective of this study is to determine O_2 consumption rates and O_2 distribution with high spatial resolution in the upper sediments along the beach infiltration zone during the seasons. We aim to investigate how seasonal inputs of O_2 and OM as well as POM retention in the sand body and regulate OC remineralization and redox zonation in the upper intertidal beach aquifer. The study contributes to the mechanistic understanding of how biogeochemical processes are regulated in intertidal sandy beach aquifers. The results add to the knowledge needed to constrain where and at what rate biogeochemical processes occur in beach aquifers. In addition, we provide a first estimation of oxic OC remineralization in the seawater infiltration zone over the annual cycle and offer a fundamental basis for future modeling approaches to further constrain the chemical boundary conditions of the biogeochemical beach reactor.

2. Materials and Methods

The study was carried out in the framework of regular field campaigns within the interdisciplinary research project DynaDeep that was recently presented by Massmann et al. (2023). In Section 4 of their publication, the authors provide a comprehensive overview of the methods that are also used in this study. Here, we present a brief summary and refer to Massmann et al. (2023) where applicable and provide additional details were necessary.

2.1. Study Site and Sampling Strategy

The field investigations for this study were performed at the meso tidal high energy beach of Spiekeroog. Spiekeroog is part of the north-western German barrier island chain that belongs to the Wadden Sea. The island faces the back-barrier tidal flats in the south and the open North Sea in the north (Figure 1a). On the northern beaches, porewater flow in the upper intertidal sand body is driven by a semidiurnal tide with a mean range of 2.7 m and mean significant wave heights of 1.4 m (Herrling & Winter 2014, 2015). The beach aquifer sediments consist of fine to medium quartz sand with a d_{50} of 200–300 μm (Beck et al., 2017) and permeabilities in the range of 6×10^{-12} to 3×10^{-11} m^2 (Grünenbaum, Greskowiak, et al., 2020). The investigated cross-shore transect in this study (Figure 1b) is part of the DynaDeep observatory (Massmann et al., 2023) and comprises 4 stations (IT 1–4) of around 10 m distance from each other in the upper intertidal part of the beach perpendicular to the mean highwater line (MHWL at 1.4 m average sea level (asl)). To cover a yearly cycle, we conducted 7 field campaigns altogether with surveys in spring (May 2022 and April 2023), summer (June and August 2022), autumn (October 2022), and winter (December 2022 and February 2023). Sampling was carried out independent of the lunar cycle, with spring tide conditions in June and October 2022, neap tide conditions in May 2022 and February 2023 and intermediate phases between spring and neap tides during August and December 2022 as well as April 2023. Except for May 2022, all samples during the campaigns were collected during one single low tide event. In May 2022, samples were taken over four consecutive days during low tide. The location of the sampling transect was chosen based on the general porewater flow induced by tidal pumping (Figures 1c and 1d). The length of the upper intertidal seawater infiltration zone at the MHWL was reported to vary between 30–70 m (Grünenbaum, Ahrens, et al., 2020). Therefore, we expected seawater infiltration into the upper saline plume of the beach aquifer to take place within our sampled zone.

2.2. Sampling Procedures and Analysis

Porewater samples were extracted in 10 cm steps down to 1 m depth along the transect during low tide using stainless steel porewater lances as described by Reckhardt et al. (2015). Porewater O_2 concentrations were immediately determined using a flow through oxygen optode (Pyroscience OXFTC) with a mobile measuring device (Pyroscience Firesting GO2). Temperature was determined by inserting the external T-sensor of the measuring device into the outflow of the flow cell. The residence time of the sampled water in the lance was less than 10 s. Contamination with O_2 was tested by drawing anoxic samples near the low water line. O_2 concentrations were below 1 μmol l^{-1}, indicating negligible contamination during the sampling procedure. Sampling was usually not possible in the first 20–30 cm depth due to the desaturation of the upper sediment layers during ebb tide. To characterize the extent of the oxic zone during each sampling campaign, the oxic portion of the transect was conservatively determined as the percentage of sampling points with an O_2 concentration above 5 μmol l^{-1}.

The temperature measurements at the flow cell were primarily used to ensure correct O_2 optode measurements. The values also represent in situ porewater temperatures, although with the limitation that conductive heat flow through the lance wall during sampling cannot be ruled out. Therefore, the temperature values obtained are presented only as mean values for each sampling campaign (Table 1) and interpreted as general indicators of in situ conditions and seasonal temperature variations.

Sediment from the locations was retrieved as described by Massmann et al. (2023) by first sampling and then removing the upper layers by hand down to 15 cm depth and thereafter by inserting a 90 cm long push core (2.54 cm diameter, AMS Stainless Steel Replaceable Tip Sand Probe). The samples were immediately transferred to the laboratory and dissected in 10 horizons: 0–5, 5–10, 10–15, 15–25, 25–35, 35–45, 45–60, 60–75, 75–90, and 90–105 cm. After each sample was homogenized, subsamples were incubated to experimentally determine O_2 consumption rates as described below in more detail. Additional subsamples for total OC (TOC) and grain size analysis were taken and frozen at −20°C until further processing. In addition, fresh samples from the upper 3

Table 1

Mean Porewater O_2 Concentrations, Anoxic Fraction, Mean Porewater Temperature (T_{PW}), and Saturation Concentration (c_{sat}) for Salinity of 32 PSU

Campaign	Mean O_2 [μmol l^{-1}]	Anoxic fraction [%]	Mean T_{PW} [°C]	c_{sat} (μmol l^{-1})
May 2022	134.9	3	17.1	247.7
June 2022	92.5	11	22.2	225.3
August 2022	76.2	0	21.1	230.0
October 2022	131.3	0	14.8	253.1
December 2022	177.4	0	6.7	309.4
February 2023	119.4	0	5.9	315.3
April 2023	170.2	0	9.4	290.8

Note. Mean values were averaged over the entire transect.

horizons at IT 3 were used to measure C and N contents of the sand fraction holding only the fine suspendable particulate matter (SPM). For this, the fine fraction of the sediments was washed out by shaking a mixture of 100 ml wet sediment and 300 ml purified water for 30 s, then allowing the suspension to settle for 10 s and filtering 100 ml of the supernatant onto 0.7 μm GF/F filters. After rinsing with 25 ml of MQ water, the filters were dried at 60°C for 24 hr and stored in a desiccator until further processing. The SPM sampling was conducted 5 times throughout the year.

Sediment samples were further processed in the laboratories of the Alfred Wegener Institute in Bremerhaven and at the Coastal Geology and Sedimentology laboratories of the Christian Albrechts University in Kiel. In preparation for TOC analysis, the frozen samples were dried at 60°C, ground and then acidified with 20% HCl to remove carbonates. Subsequently, 500 mg were measured in a CS analyzer (Eltra CS 800). The measurements detection limit was 0.00012 weight (wt.) % C in a sample with a precision of 0.0005 wt. %. The SPM filters were acidified and the C and N content was measured in a CHNSO analyzer (Hekatech Euro EA). For grain size analysis, dried samples (60°C) were sieved with a mesh size of 2 mm to discard shell debris. The sand particles were analyzed using a Sympatec QICPIC analyzer. In this, a high-speed camera (100 Hz) captures individual particle images of a free falling 15 ml subsample. Image analyses result in particle size and shape distributions.

2.3. Beach Topography

The beach topography was acquired using digital elevation models (DEMs) derived from aerial imagery and manual real-time kinematic (RTK) differential GPS-surveys. A drone captured aerial images (Figure 1-b) from an altitude of 80 m at low tide, when the intertidal area of the beach was visible. Each collection of aerial pictures comprised a range of 300–600 high-resolution photos, which were combined using a photogrammetry software (Massmann et al., 2023). During the campaigns for this study, the coordinates of the sampling locations IT 1–4 at the transect were determined by differential GPS measurements (Stonex S9 III Plus GNSS), and the topographic information for the transect was derived from the DEMs using the sampling locations. During unfavorable weather conditions that prevented drone flights, as experienced in December 2022, the beach profile was instead measured using differential GPS measurements only.

2.4. Sedimentary Incubation Experiments

Slurry incubations were set up to experimentally determine O_2 consumption rates. Experiments were carried out in the laboratories on Spiekeroog directly during the respective sampling campaign. In short, gas tight vials (Labco Exetainer® 12 ml) equipped with O_2 sensor spots (Pyroscience, OXSP5) were filled with sediment (6–8 ml) and carefully topped with 0.2 μm filtered air-saturated seawater, leaving no gas phase in the vial. To mimic in situ conditions, the vials were incubated in the dark at in situ temperatures. To induce porewater advection, the incubation vials were mounted on a slowly rotating wheel ensuring a gentle and continuous exchange between sediment and water phase. This approach prevents stagnation of O_2 transport and related O_2 limitations of the consumption rates. Sediments were incubated in duplicates (some triplicates in August 2022) and 4–13 O_2 measurements (i.e., readings of O_2 sensor spots) were carried out in regular intervals over a timespan of up to 25 hr, depending on the rate of O_2 consumption. We performed a linear regression analysis on the measured O_2

concentrations over time and calculated the O_2 consumption rate per volume porewater from the slope, considering dilution by excess water at a sediment porosity (Φ) of 0.34 (determined from salinity breakthrough curves in flow through reactors, unpublished data). Filtered seawater incubated without sediment served as control experiments, and the blank rates (average of 0.7 ± 0.2 μmol l^{-1} h^{-1} across all campaigns, Table S1 in Supporting Information S1) were subtracted from the calculated rates. The lowest rate determined by our method was 0.2 μmol l^{-1} h^{-1} in April 2023 at IT1 at 90–105 cm depth, indicating the detection limit of the method. For all rate measurements, the significance level of the linear regression was set to $p \leq 0.05$ except for some measurements in Winter (December 2022 and February 2023), where $p \leq 0.2$ was used to allow an estimate of the very low rates. The significance of these rates emerges from the overall view of the entire profiles, where a high degree of reproducibility was found. Rates above the respective significant levels were treated as nonsignificant.

In many studies, O_2 consumption rates in permeable sands have been measured under controlled advective conditions using flow through reactors (FTRs) (e.g., Ahmerkamp et al., 2020). During two campaigns, FTR incubations and slurry incubations were carried out simultaneously and showed comparable results (Massmann et al., 2023). The slurry incubations provide a novel high-throughput approach that is necessary to simultaneously measure O_2 consumption rates in multiple samples from several depths.

2.5. Flux Estimations

The measured volumetric O_2 consumption rates were integrated over the respective sampled horizon depth d_H and summed up to obtain O_2 fluxes (Flux$_{station, O2}$) per m^2 at each sampling location (Equation 1). For a C flux estimate into the entire seawater infiltration zone (Flux$_{IT, C}$), O_2 fluxes were converted to OC fluxes. We assumed a respiration quotient C:O_2 of 106:138 for the oxidation of organic material with a C:N ratio of 106:16 (Redfield et al., 1963), taking into account 106 mol O_2 for the oxidation of OC and 32 mol O_2 for nitrification. We then considered the distance between sampling locations of about 10 m and conservatively assumed that each of the stations represents 10 m of a 40 m cross-shore infiltration zone with O_2 generally available in the upper meter. This yields Equation 2. In summary, Flux$_{IT, C}$ represents an estimation of the total OC turnover in a 40 m long oxic seawater infiltration zone down to one m depth and per meter shoreline. Flux$_{station, O2}$ and Flux$_{IT, C}$ were calculated for every sampling campaign.

$$Flux_{station,O_2}\left[\frac{mmol\ O_2}{m^2 * d}\right] = \sum_{H=1}^{10} R_H\left[\frac{mmol\ O_2}{m^3 * d}\right] \cdot \Phi \cdot d_H[m] \tag{1}$$

$$Flux_{IT,C}\left[\frac{g\ C}{m * d}\right] = \sum_{station=1}^{4} Flux_{station}\left[\frac{mmol\ O_2}{m^2 * d}\right] \cdot 0.77\left[\frac{mmol\ C}{mmol\ O_2}\right] \cdot 12\left[\frac{g\ C}{mmol\ C}\right] \cdot 10\ [m] \tag{2}$$

To compare the seasonal carbon fluxes Flux$_{IT, C}$ with the availability of fresh organic matter in the seawater and with seawater temperature, we determined the monthly averages of carbon bound in phytoplankton, Phy-C as mmol C m^{-3}, and temperature, T in °C from a biogeochemical and physical ocean model for the European North West Shelf, respectively (E.U. Copernicus Marine Service Information (CMEMS), 2023, 2024). The data covered our investigation period (May 2022–April 2023) and considered the adjacent North Sea area between 53.7–54.5°N and 7.2–8.2°E.

2.6. Data Analysis and Presentation

Data below the detection limit of our methods were set to 0. To analyze functional relationships, the Python v3.9.7 libraries Numpy and Scipy were used. The obtained data sets for O_2 concentrations and O_2 consumption rates were combined with the beach profiles to create contour plots using Python's v3.9.7 libraries Numpy, Pandas, Scipy, and Plotly. The plots depict the analyzed transect along the UTM 32U easting coordinate with the northing values of 5959880–5959950 (x-axis). The plots additionally show the distance to the mean high water level (MHWL) at 1.4 m above average sea level, indicating the location of the sampled transect in the intertidal zone. For presentation, the data were extrapolated over 3 m along the x-axis from the uppermost (IT 1) and lowest (IT 4) sampling location, respectively. In the O_2 distribution contour plots, O_2 concentrations were extrapolated to the respective minimum sampling depth per campaign using nearest neighbors. Between sampling points, the data
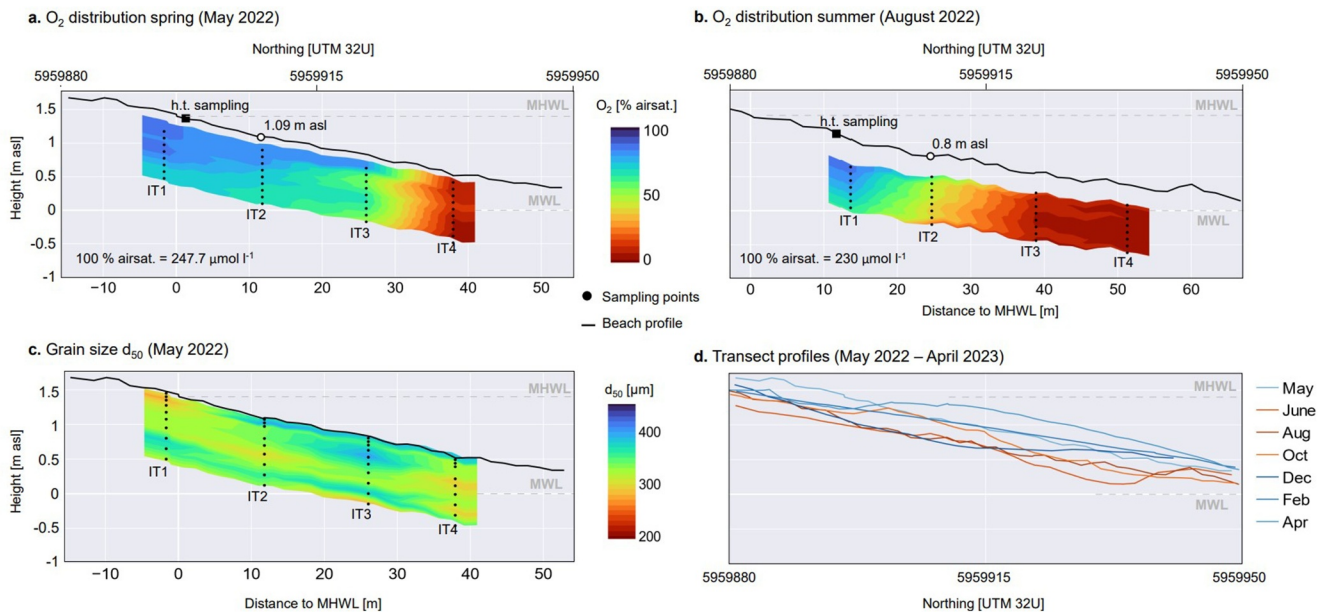
Figure 2. (a and b) Spatial O_2 distribution in % air saturation during an exemplary spring and summer campaign at the transect along the easting coordinate with the northing values of 5959880–5959950, shown as colorcode. As a reference, the O_2 concentration at 100% air saturation for the respective survey's mean T is given in the bottom left corner of the subplot. The position of the high tide (h.t.) level prior to sampling is shown as a black square. In May 2022, sampling was conducted on four consecutive days, and the position of the high tide level preceding sampling at IT 1 is marked. To demonstrate sediment deposition and erosion, the height of the beach profile at IT2 (northing value 5959907) is shown. (c): Distribution of median grain size (d_{50}) at the transect along the easting coordinate in May 2022 shown as colorcode. (d): Profiles of beach topography at the transect during all 7 sampling campaigns from May 2022–April 2023. Winter and spring profiles in more so-called dissipative morphodynamics in blue, summer and autumn profiles with more so-called reflective behavior in orange.

points were linearly interpolated on a rectangular grid with the depth below the beach surface on the *y*-axis. The y-coordinates of these interpolated data points were then shifted to positions relative to average sea level.

3. Results

3.1. Oxygen Distribution

The seawater that infiltrates into the beach aquifer comes from well mixed surface waters, so we expect O_2 concentrations close to air saturation. Hence, oxic porewater indicates the physical location of infiltrated seawater that has not yet exceeded the residence time for complete O_2 depletion. During the first sampling campaign in May 2022, we found that the sampling transect comprised the upper oxic infiltration zone with the highest O_2 concentrations at IT 1 near the MHWL and a transition to low O_2 concentrations at IT 4 closest to the MWL (Figure 2a). This pattern was found throughout the year, indicating that O_2 intrusion due to infiltrating seawater and the general flow pattern along the transect remained unchanged during the yearly cycle (Figure S1 in Supporting Information S1). Mean O_2 concentrations at each sampling station were lowest at IT 3 and 4, ranging from 13.1–147 μmol l^{-1} at IT 3 and 10.9–135 μmol l^{-1} at IT 4 throughout the year. Over the seasons, there was a trend of further decreasing O_2 concentrations along the transect in summer (Figure 2b), with the lowest mean O_2 concentrations (averaged over the sampling transect) in the summer months, and increasing O_2 concentrations toward winter and spring (Table 1). Oxic conditions ($O_2 > 5$ μmol l^{-1}) prevailed throughout the year. Anoxic conditions were observed only in May and June, occurring in 3% and 11% of the samples, respectively (Table 1). These anoxic conditions were limited to sampling points IT 3 and 4 (Figure S1 in Supporting Information S1). The mean porewater temperature followed the seasonal trend with maximum values in summer. In addition, the seasonal trend in temperatures determined the O_2 concentration of air saturated seawater (Sal = 32 PSU) and thus the seasonal input of O_2 into the infiltration zone (Table 1).

3.2. Beach Sediments and Morphodynamics

In May 2022, sediments at the transect consisted of medium sand with a median grain size d_{50} of 275–400 μm and variations in stratigraphy (Figure 2c), which did not experience large changes despite topographic changes over

the summer (Figures S2b and S2c in Supporting Information S1). The topography of the investigated beach transect exhibited slopes of 0.5%–2.4%, with sediment height varying by up to 65 cm over the course of the year (Figure 2d). Nevertheless, topography changes between the individual campaigns were in the range of a few decimeters. When comparing the height of the intertidal zone at UTM 32U northing 5959907 as a representative intertidal point at the transect (Figure S1 in Supporting Information S1), the height of the sediment changed by a maximum of 31 cm from December to February. From winter to spring (Figure 2d), we observed a so-called dissipative morphodynamic state, which typically develops under higher wave energy conditions with a wider surf zone and gentler slopes along the intertidal zone (Wright & Short, 1984). No distinguishable morphological features were observed in this state during our investigations. In contrast, profiles measured from June to October showed a so-called reflective behavior with slightly steeper slopes in the upper intertidal and ridge-runnel systems.

3.3. Oxygen Consumption Rates

Volumetric O_2 consumption rates at all sampled transects ranged from below 0.2 to up to 106 µmol l^{-1} h^{-1} (Figure 3) with minimum values in February and December (Figures 3e and 3f) and maximum values in June and August (Figures 3b and 3c). The spatial distribution of rates at the transect exhibited a vertical gradient throughout the year. During all campaigns, the rates in the first decimeters were higher than the rates further below (*t*-test p-value <0.05 when comparing rates in the upper 20 cm and rates below, see also Figure 4). In May and June (Figures 3a and 3b), we observed the strongest vertical gradient of rates over depth. This effect was most pronounced at IT 1 in June with rates in the upper 5 cm of 106 µmol l^{-1} h^{-1} and a 40-fold decrease with depth to 2.4 µmol l^{-1} h^{-1}. Notably, in August (Figure 3c), we found that the rates below the first decimeters were above those measured at previous months (Figure 3c), and a particularly high rate of 52 µmol l^{-1} h^{-1} was measured at a depth of 90–105 cm at IT 4. During winter (Figures 3e and 3f), the rates declined again, with a maximum rate of 11 µmol l^{-1} h^{-1} in December at a depth of 5–10 cm at IT2, whereas rates in deeper parts were mostly around 2–3 µmol l^{-1} h^{-1}.

Interestingly, we observed secondary peaks of rates in June (up to 42 µmol l^{-1} h^{-1} at IT 2 at 15–25 cm), August (up to 47 µmol l^{-1} h^{-1} at IT 4 4 at 15–25 cm), and October (up to 37 µmol l^{-1} h^{-1} at IT 3 at 25–35 cm) (Figures 3b–3d). In two cases, the secondary peaks were located on the beach profile of the previous campaign as indicated by the dashed line in Figure 3, suggesting sediment deposition between the successive campaigns. From June to August (Figure 3c), we found a deposition of 23 cm at IT 4, and from August to October (Figure 3d), we found a deposition of 16 cm at IT 3. Such secondary peak rates were local and singular features with an apparently short lifespan, as they have never been observed repeatedly in consecutive campaigns. Effects of sediment erosion, such as a lack of elevated rates in the upper filtration layer, were not evident.

The rate profiles at all 4 locations (IT 1 to IT 4) were similar for each campaign, so that average rates pooled per sampling depth (horizon) were calculated for the different months (Figure 4). The obtained rate profiles clearly illustrate the seasonality of O_2 consumption rates in the upper beach meter. The rates in winter are low at all depths, then the rates in the top filtration layer start to increase in spring and early summer. At greater depth an increase of rates is clearly observed, but it lags behind the rate increase at the top and peaks in late summer (August) where the top rates are already in decline. In autumn, the rates have already declined across the entire depth profile and further continue to decline until winter.

By further integrating the rate profiles over depth, the seasonality of the oxygen uptake per m^2 was calculated (Equation 1). The oxygen uptake was low in winter with an average flux at the sampling stations of 22 mmol O_2 per m^2 and day in December and February and increased by a factor of 8 in summer to peak at 186 mmol O_2 per m^2 and day in August (Figure 6). In C equivalents, assuming a respiratory quotient C:O_2 of 0.77 (Redfield et al., 1963), the estimated mineralization varied between 15 (winter) and 143 (summer) mmol C m^{-2} d^{-1} with a yearly average of 73 mmol C m^{-2} d^{-1}.

3.4. Organic Carbon Content

TOC content of the sampled sediments ranged between 0.004 and 0.024 wt. % with an average of 0.009 wt. % (measurements detection limit 0.00012 wt. %, see also Section 2.2). Figures 5a–5g shows the TOC profiles averaged over the 4 sampling locations (IT-1 to IT-4) for the campaigns. We did not observe a trend in TOC content with depth or seasons. The most striking result is that we also did not observe a correlation of TOC
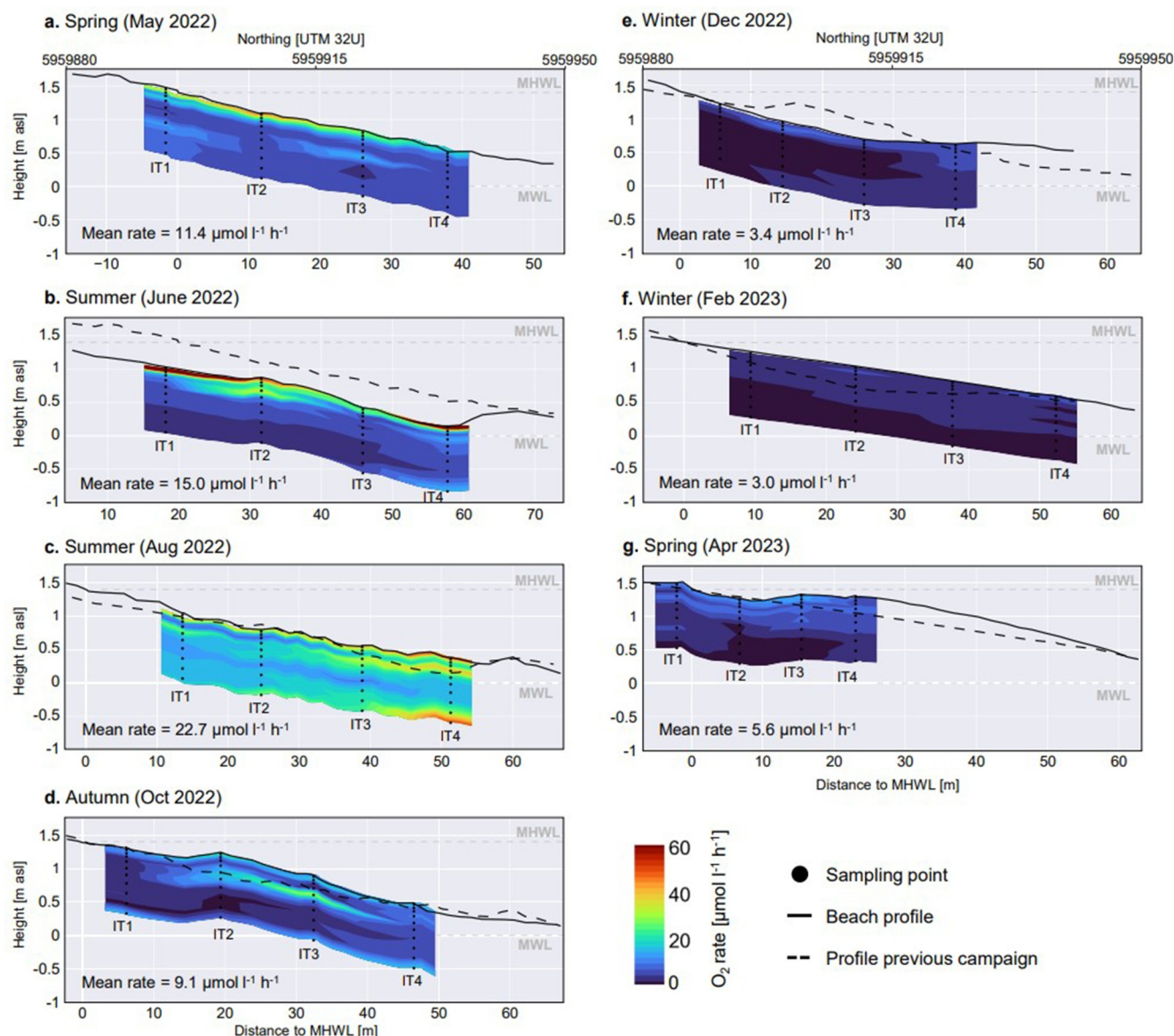
Figure 3. Spatial distribution of O_2 consumption rates along the easting coordinate with the northing values of 5959880–5959950 during the seven separate sampling campaigns (a–g). In addition, the mean rate across all samples per survey is given in the bottom left corner of each subplot. Measured beach topography during sampling (solid profile) as well as profile of previous campaign (dashed profile) are indicated to show topography changes between campaigns.

contents with the O_2 consumption rates (compare Figures 4 and 5). The retention of particulate OC (POC) in the upper decimeters and the seasonal variation of seawater POC loading is not reflected in the bulk TOC contents. However, the suspendable fine fraction of the upper 15 cm, which constitutes only around 0.01 weight % of the sediment, was more than 100-fold enriched in OC (Figure 5h) and showed a clear seasonal trend with rising mean contents from winter to summer and declining in autumn. To connect the OC content in the fine fraction to the bulk wet sediment, we extrapolated the measured OC in the filtered 100 ml to the total volume of water used for washing out the fine fraction (at a sediment porosity of 0.34) and related it to the analyzed sediment volume (see Section 2.2). Average OC remineralization rates per volume wet sediment in the top 15 cm at IT-3, calculated from O_2 consumption rates assuming a respiratory quotient $C:O_2$ of 0.77 (Redfield et al., 1963) and sediment porosity of 0.34, were directly correlated with the average fine OC content of the sediment (slope = 0.015 hr^{-1}, $R^2 = 0.97$, Figure 5i).
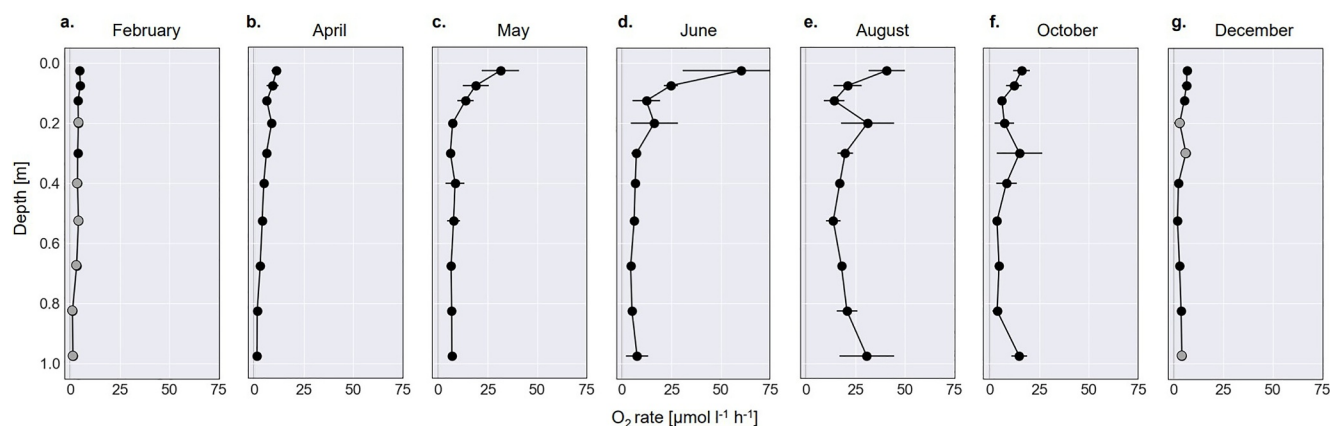
Figure 4. O$_2$ consumption rates averaged per sampling depth (horizon) across the 4 sampling locations (IT 1 to IT 4) during the seven separate sampling campaigns (a.)—(g.), error bars show the standard deviation of all measurements per depth horizon, usually composed of $n = 8$ incubations. Data points marked in gray indicate that of these 8 measurements some rates were not significant and thus were disregarded when averaging. For February, the number of data points (out of $n = 8$ samples) that were used for averaging is: 7 for 25–35 cm and 35–45 cm, 6 for 45–60 cm, 5 for 90–105 cm, and 2 for 60–75 cm and 75–90 cm. For December, these statistics are: 6 for 75–90 cm, 5 for 15–25 cm, and 2 for 25–35 cm.

3.5. Carbon Fluxes

The amount of OC that is remineralized via oxygen respiration was integrated over the entire upper meter and over an estimated 40 m long oxic beach infiltration zone. The estimated C fluxes varied by a factor of 10 from about 5 g C per m shoreline and day in the winter to 69 g C m^{-1} d^{-1} in summer (Figure 6). In the course of the year, fluxes remain below 15 g C m^{-1} d^{-1} from winter to spring with lowest values from December to February and doubling from February to April. After April, the flux increases more rapidly, peaking in summer. From summer to autumn, the flux decreased by more than 60% before bottoming out again in winter. Integrating the fluxes for the entire year results in 9.5 kg of C being remineralized per m shoreline of which 7 kg are turned over just in the months June to October. Throughout the year, changes in phytoplankton-bound C concentrations in the specified Spiekeroog North Sea area followed the vegetation season (Figure 6). Values ranged from 2 mmol C m^{-3} during the winter to a peak of 17.5 mmol C m^{-3} in the summer. The minimum values were consistently recorded during December and January. Seawater temperature ranged from 5.6°C in February to 19.2°C in August, following the seasons. C fluxes correlate exponentially to phytoplankton-bound C ($R^2 = 0.93$, Figure S4a in Supporting Information S1) and seawater temperature ($R^2 = 0.92$, Figure S4b in Supporting Information S1).

4. Discussion

Common approaches to study biogeochemical reactions in beach aquifers include the measurements of in situ porewater concentrations (Ahrens et al., 2020; Charbonnier et al., 2013, 2016; Reckhardt et al., 2015) next to a combination of assumed boundary conditions and model-based transport rates (e.g., Greskowiak et al., 2023; Kim et al., 2020; Spiteri et al., 2008) from which reaction rates can be concluded, if not already assumed apriori. In this study, however, we directly measured the sedimentary O$_2$ consumption rates at high spatial resolution and throughout ayearly cycle using novel high-throughput slurry incubations. This allows, for the first time, to resolve spatial and seasonal changes in sedimentary reaction rates, which are necessary to understand and quantify the effects of changing boundary conditions on the beach bioreactor. Combined with measurements of sedimentary OC content, O$_2$ distribution, and beach topography, we interpret the O$_2$ consumption rates in light of seasonal changes in temperature, O$_2$ and OM availability, together with morphodynamics and the sand filtration efficiency for POM. We also investigated how this affects OC remineralization and redox zonation in the upper meter of a beach infiltration zone.

4.1. Oxygen Consumption Rates

In this study, we provide a unique high resolution data set of O$_2$ consumption rates from sediments in the intertidal beach aquifer measured throughout an entire year and under realistic conditions (Figures 3 and 4). The measured rates of 0.4–106 µmol l^{-1} h^{-1} are between the few reported O$_2$ consumption rates from the Delaware Beach Aquifer (Kim et al., 2017, 2019) and the Iberia Beach Aquifer (Ibánhez & Rocha, 2016). However, a comparison
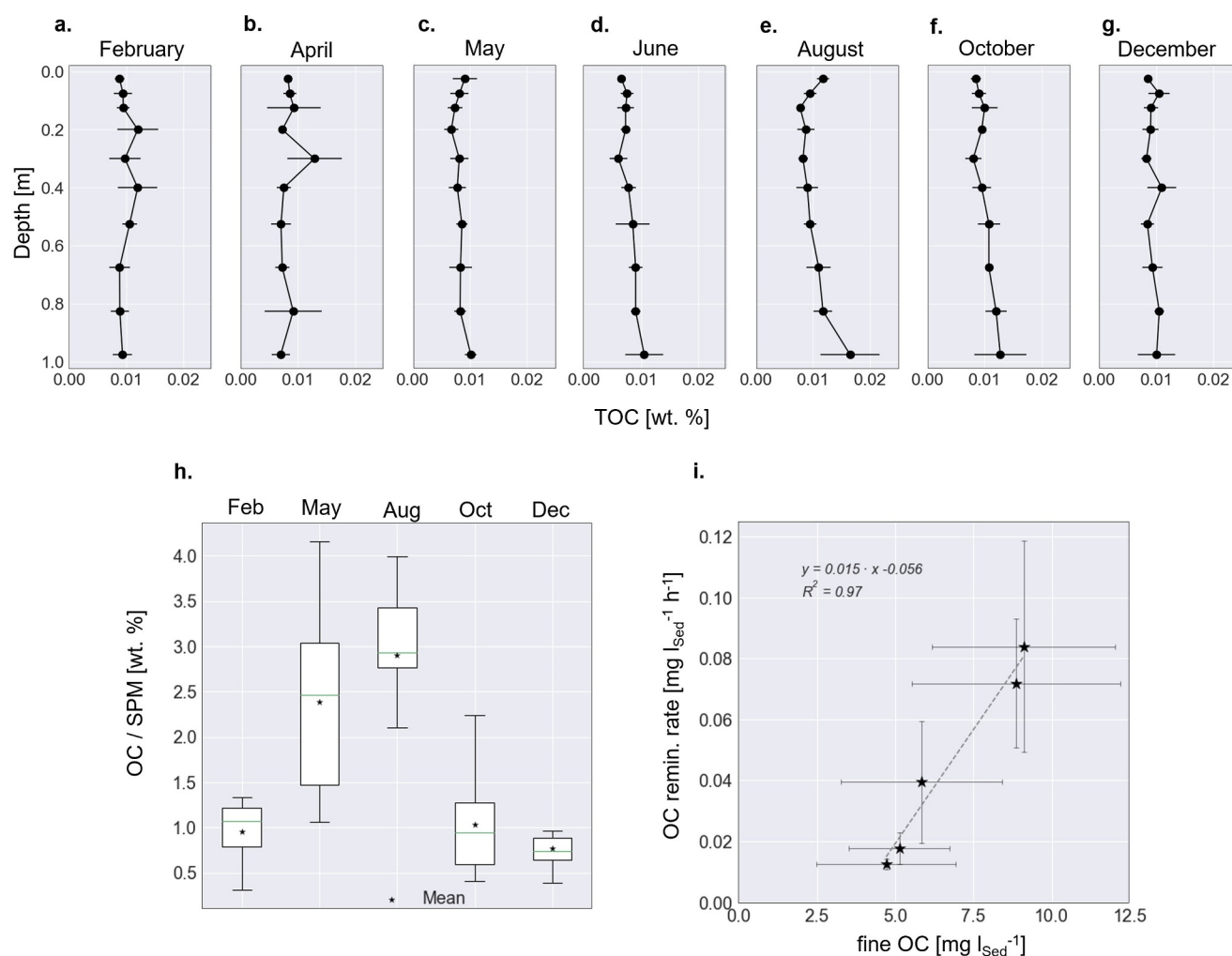
Figure 5. (a–g): Bulk sedimentary TOC content pooled per depth across the 4 sampling locations (IT 1 to IT 4), error bars show the standard deviation of all samples per depth horizon; (h): OC content per suspendable particulate matter in the top 15 cm at IT3 throughout the year. Boxplot shows median value of all samples (0–5, 5–10 and 10–15 cm horizons) as green line, first and third quartile as box, minimum and maximum values as whisker and mean value as star; (i):. Average OC remineralization rates are directly correlated to average fine OC content ($R^2 = 0.97$) in the top 15 cm at IT 3, error bars show the standard deviation of all samples.

is difficult as the high rates of Ibánhez & Rocha (30–187 μmol l^{-1} h^{-1}) were measured in the exfiltration zone, whereas Kim et al. (2017) incubated porewaters (without sediments), reporting very low rates of 0–0.13 μmol l^{-1} h^{-1}. In another study, Kim et al. (2019) presented a few incubations from the same location that included the sediments fraction and found significantly higher rates of 0.4–3.2 μmol l^{-1} h^{-1}. This confirms the findings of Probandt et al. (2018) that the microbial community in sands is particularly abundant on sand grain surfaces as well as the findings of Ahmerkamp et al. (2020), who showed that bulk O_2 consumption rates scale with the grain surface area and corresponding cell density.

When designing incubation experiments with permeable sand, considering advective pore water flow is indispensable. Without sufficient advective flow, O_2 limitation of the microbial community on the sand grains may occur, leading to the formation of microenvironments in poorly flushed areas and inaccurate rate determinations (Ahmerkamp et al., 2020). Rate measurements are therefore often performed using flow through reactors (FTRs) (e.g., Ahmerkamp et al., 2020; Ibánhez & Rocha, 2016), which were also carried out during the field campaigns in this study. However, FTR incubations were not feasible at the targeted spatial resolution of 40 dublicate incubations per campaign. Therefore, we developed slurry incubations, which ensure porewater flow and compare well to rate measurements in FTRs (Massmann et al., 2023), while allowing for numerous simultaneous rate measurements.
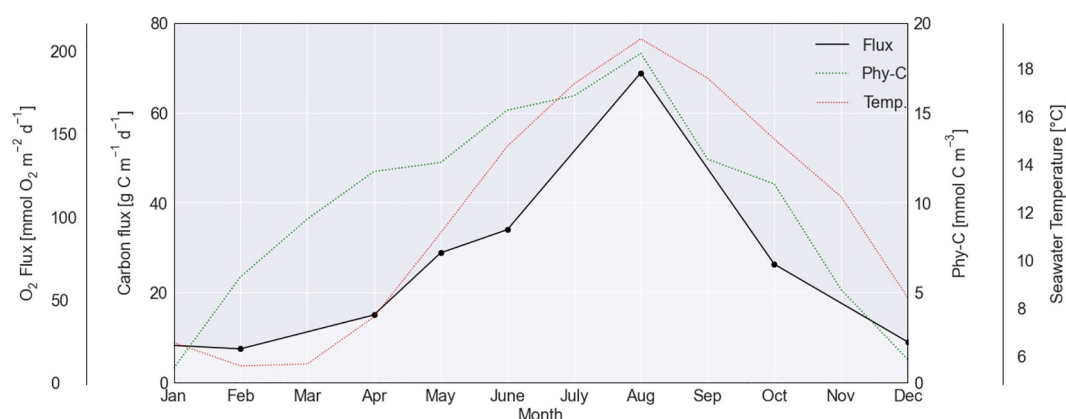
Figure 6. Yearly cycle of measured O_2 fluxes presented as the average of the 4 sampled stations per square meter and day (outer left scale). Yearly cycle of calculated C flux for the 40 m long beach infiltration zone per meter of shoreline and day (inner left scale). The dotted green line shows concentrations of C bound in Phytoplankton (inner right scale) and the dotted red line the temperature of seawater (outer right scale) derived from respective biogeochemical and physical ocean models for the European North West Shelf (E.U. Copernicus Marine Service Information (CMEMS), 2023, 2024).

During the slurry incubations, a gentle movement of the porewater prevented O_2-limitation of reaction rates. However, under in situ conditions, porewater flow in the field may be reduced to stagnant conditions during full immersion at high tide. At stagnant conditions, the O_2 consumption could lead to O_2 depletion over time, depending on the available O_2 concentration and the reaction rate. In this case, the experimentally derived rates would overestimate the in situ rates. However, during the O_2 measurements in the field, we did not detect O_2-depletion except for the reported 3% and 11% of anoxic samples in May and June, respectively (Table 1). Because the O_2-sampling took place at low tide, it is possible that some of the locations with low O_2 became O_2-depleted during stagnant conditions at high tide. We found that this is a possible scenario only at the lowest sampling stations, IT 3 and 4, because of prolonged immersion periods and low O_2 concentrations (Figure S1 in Supporting Information S1). During the warmer months (May–October), locally elevated rates at some depths could have depleted the low O_2 concentrations within 1–2 hr. However, such possible depletion was found only for 6% of the overall samples. In addition, such temporary anoxia would be short-lived, occurring only during a part of the temporary stagnant conditions at high tide. We therefore conclude that the experimentally determined rates provide a reasonable basis to estimate daily fluxes for the 40 m long, 1 m deep oxic infiltration zone.

In principle, elevated O_2 consumption rates during the incubation could also steem from reoxidation of reduced compounds, such as Fe(II)-bearing minerals (Zhou et al., 2023). Lowest mean O_2 concentrations were found in August, where the O_2 concentrations along the transect were decreased compared to June (Figures S1b and S1c in Supporting Information S1). Although the bulk redox conditions were oxic (Table 1), some anoxic niches may have formed where reduced compounds could have accumulated. However, a possible rate-bias due to reoxidation of reduced compounds should have significantly increased from location IT 1 to 4 along with the decrease of O_2 concentrations. This was only the case for the 2 samples below 75 cm at IT 4 (Figure 3c), so that we assume such a rate-bias of minor importance. This result additionally underscores that oxic conditions consistently prevailed at the four stations throughout the seasons and tidal cycle, and that O_2 consumption rates were not limited by O_2 availability.

When comparing O_2 consumption in the sandy beach in this study to the subtidal sandy sediments of the North Sea, it is evident that the infiltration zone of the intertidal beach aquifer is a high-throughput system. The volumetric O_2 consumption rates in the upper beach decimeters (Figures 3 and 4) are in a similar range to those of subtidal North Sea sands with a comparable grain size of $d_{50 >}$ 250 μm (Ahmerkamp et al., 2017), which were determined by FTR rate measurements, a method comparable to our approach, as described above. However, the calculated O_2 fluxes in summer of up to 186 mmol per m^2 are 5–23 times higher than fluxes of 8–34 mmol O_2 m^{-2} d^{-1} reported by Ahmerkamp et al. (2017). The high O_2 fluxes are the result of the deep O_2 penetration depth of over 1 m (Figure 2 and Figure S1 in Supporting Information S1) compared to just a few centimeters in subtidal sands. The high volume flows of seawater through the infiltration zone under high-energy conditions (McLachlan & Turner, 1994) lead to a high O_2 supply and thus promote the extensive consumption of O_2 in sandy beaches.
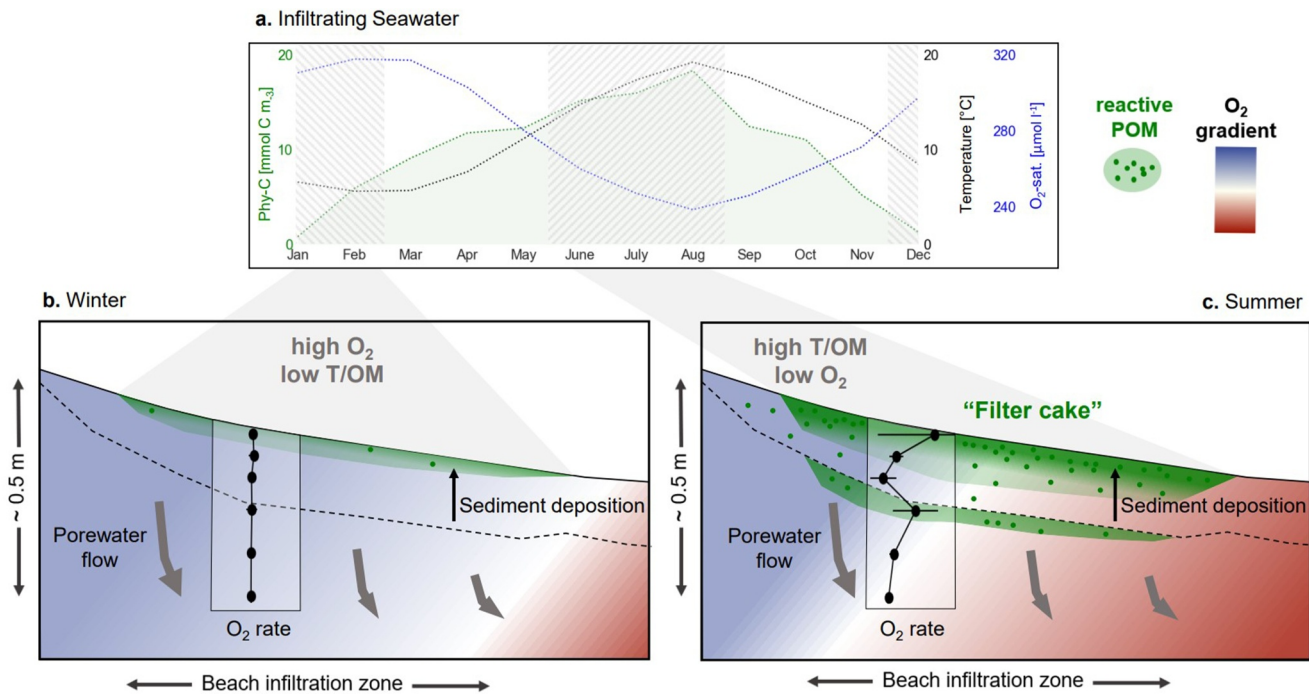
Figure 7. Concept of the mechanisms that determine seasonal O_2 consumption rates and O_2 distribution. The seasonal variations in Phytoplankton-C and Temperature as derived from the E.U. Copernicus Marine Service Information (CMEMS) (2023, 2024) also presented in Figure 6, and the resulting saturation concentration of O_2 (Garcia & Gordon, 1992) are shown in the upper panel. (b and c): The seasonal variations in infiltrating seawater drive the O_2 consumption rates, which are shown as an example as upper 40 cm of the measured rate profiles from February for winter and August for summer (Figures 4a and 4e). Efficient POM filtration and morphodynamics control the vertical distribution of rates. The O_2 distribution, shown as colored O_2 concentration from oxic (blue) to anoxic (red), is the result of porewater flow paths and the seasonal O_2 input and consumption.

Our calculated O_2 fluxes can be considered conservative estimates as we could not resolve the oxycline and thus could not integrate the volumetric consumption rates over the entire oxic sediment layer.

Assuming that O_2 consumption is primarily due to microbial aerobic degradation of organic matter, the distinct seasonal pattern of mean O_2 consumption rates (Figure 2) and the low TOC contents suggest that microbial activity in the beach sediment is impaired by the limitation of organic matter. Regulated by the seasonal changes in organic matter supply but also temperature (Figure 6), microbial activity significantly increases in the summer months. Additionally, the observed seasonal depth dependency of O_2 consumption (Figures 3 and 4), with the highest rates constrained to the upper decimeters, indicates an efficient retention of highly reactive POM within the upper layer of beach sediments. This is most pronounced in late spring and early summer (Figures 3a–3d). Our findings confirm results of a preliminary investigation of sedimentary O_2 consumption rates at our field site from 2017 (Figure S3 in Supporting Information S1), demonstrating the general validity of the observed mechanism. A so-called "filter cake" develops, comparable to the phenomena in technical filtration systems, and heterotrophic bacteria thrive on the freshly supplied matter that gets retained in the sand (Figure 7). Similar phenomena have been observed in a sandy beach aquifer in Portugal within the upper decimeters of the seepage face (Ibánhez & Rocha, 2016), and model results have suggested the presence of a pool of POM in the shallow beach beneath the infiltration zone (Kim et al., 2020). Due to the high resolution rate measurements in our study, we are now able to highlight the profound effect of POM retention on O_2 consumption in the beach infiltration zone over a complete seasonal cycle.

Our findings confirm that the vertical heterogeneity of O_2 consumption rates increases from winter to summer (Figures 4a–4-d) when elevated marine biological production increases POM concentrations in sea water. Intriguingly, we found that the horizontal heterogeneity throughout the infiltration zone is of minor importance, so that a single depth profile of averaged samples per horizon is representative for the entire infiltration zone (Figure 4). This is also confirmed by the sediment distribution, which varied little horizontally (Figure S2 in Supporting Information S1). The mean O_2 consumption rates peaked in August, when the reactivity increased significantly also in the deeper layers of the investigated sediments (Figure 4e). This increase was not attributed to temperature, as there was no change in pore water temperature between June and August (Table 1). Instead, as

previously reported, the high turnover of POM in the upper layers may lead to an increased release of dissolved OM (DOM) (Seidel et al., 2015), which is transported to deeper layers and then presumably adsorbed onto sediment grains (Zhou et al., 2024), thereby stimulating the activity of the attached microbial community.

Morphodynamics also influence the spatial distribution of O_2 consumption rates. The upper layer, exhibiting high O_2 consumption rates due to retained POM, is subjected to sediment erosion and burial. In some instances, where the topography measurements reveal sediment deposition between campaigns, the previous depth horizon was associated with a secondary peak of O_2 consumption (Figures 3c and 3d), pointing toward a short-term storage of reactive OM of the former upper layer. In our study, we did not observe the morphodynamics between the sampling campaigns, so that the exact timing and rate of the sediment deposition remains unknown as well as possible erosion events in between. However, despite the significant changes in topography between the campaigns and the assumed high morphodynamics in general, the vertical gradients of reaction rates in summer are very consistent in time and reveal a high similarity along the infiltration zone, indicating a rapid adaptation of POM retention and O_2 consumption to the changed topography. When sediment deposition leads to POM burial, we therefore assume a fast drawdown of such a POM storage accompanied by a decline in rates. On the timescale of months that we observed, correlations between previous upper layers and secondary rate peaks were found only between two consecutive campaigns, highlighting the short lifespan of buried POM. Conversely, previous sediment erosion appears to result in even faster reformation of POM retention with associated high O_2 rates, as we did not observe a discontinuation of the upper rate gradients in any case. The findings are similar to a previously described "C memory effect", which suggests a heterogeneous distribution of reaction rates in intertidal beach aquifers caused by the interplay of entrapped C and hydrological shifts (Kim et al., 2019). In our study, however, this effect was not found below 50 cm depth, suggesting a short lifespan of the buried POM, which restricts the supply of reactive POM to deeper layers by this mechanism.

Our findings suggest that seasonal changes in O_2 consumption, together with seasonal O_2 input through infiltrating seawater, regulate O_2 concentrations at the transect (Table 1 and Figure S1 in Supporting Information S1). Tidally driven inflow of oxic seawater, which can be assumed to be at air saturated concentrations, takes place between the MHWL and MWL, agreeing with modeled porewater flows in this beach section (Grünenbaum, Greskowiak, et al., 2020). The size of the infiltration zone is around 40 m, aligning well with previous findings of 30–70 m length (Grünenbaum, Ahrens, et al., 2020). Grünenbaum, Ahrens, et al. (2020) reported average infiltration velocities of 0.21 ± 0.13 m d^{-1} in the sampled zone, highlighting the high variability in porewater flow. Typically, vertical velocities in the infiltration zone are highest at the HWL and decrease further down the beach, fluctuating over the tidal cycle (Robinson et al., 2007). However, in contrast to tidal variations, Charbonnier et al. (2016) found that seasonal changes had a stronger influence on the distribution of porewater O_2, which supports our findings. Nevertheless, factors such as spring-neap tidal cycles (Heiss & Michael, 2014) and morphodynamics along the beach have a direct impact on porewater velocities. This in turn influences the extent of the oxic zone and determines where O_2 is microbially available. In this study, we did not resolve the extent of the oxic zone, which is substantially larger than the sampled upper meter (Reckhardt et al., 2024). Based on our findings, a strong impact by these factors on O_2 consumption can be expected in the deeper beach reactor especially close to the oxycline, where O_2 availability is directly influenced. However, the consistent O_2 abundance found in the upper layer indicates sufficient O_2 supply by the infiltrating seawater, so that the variations in porewater transport are expected to have a negligible effect.

Mixing with fresh anoxic groundwater can be assumed negligible in the upper subsurface of the infiltration zone (Figures 1c and 1d). Therefore, porewater O_2 concentrations below saturation concentration indicate consumption of O_2 due to aerobic respiration after infiltration, which is the case along the entire transect in spring and summer (Figure S1 in Supporting Information S1). The O_2 distribution generally shows a horizontal gradient. As vertical porewater velocities are expected to decrease along the transect, lower O_2 concentrations at the lower parts correspond to longer residence times. However, vertical O_2 gradients were not strongly pronounced, suggesting that flowpaths are not strictly vertical but also oriented along the horizontal beach topography. Such reorientation of flow paths along the transect could be caused by changes in hydraulic conductivity with depth or flow direction (anisotropy) as well as by influences of morphodynamics such as ridge-runnel systems. Although a complete assessment of porewater flow was beyond the scope of this study, we would like to point out that the comprehensive measurement of both the concentration and the consumption rates of a reactive tracer, such as O_2, can provide valuable information about flow direction and magnitude.

4.2. Carbon Dynamics

The TOC content of the beach sediment in the infiltration zone is in the lower range of values reported for sandy beach sediments (<0.01 wt% (Anschutz et al., 2009) to < 0.08 wt% (Ibánhez & Rocha, 2016)) and does not indicate an accumulation of C neither in the top layer nor during the summer months (Figure 5a–5d). However, this counterintuitive result is characteristic of sandy sediments, indicating a rapid turnover of OC (Rocha, 2008). Our results emphasize that a low OC stock does not mean that beaches are biogeochemical "deserts" but, on the contrary, that the OC supplied is rapidly consumed due to the high influx of O_2 (Boudreau et al., 2001). Notably, we did not observe higher TOC values in the upper sediment decimeters, which could have been expected due to POM retention. Thus, TOC content in sandy sediments is not a good indicator for the microbial activity therein. A previous study from the Delaware Beach aquifer (Kim et al., 2019) also found no correlations between depth, organic matter content, grain size (Figure S2 in Supporting Information S1), and respiration rate. Other studies reported only subtle changes of TOC content over the season or with depth (Calvo-Martin et al., 2021; Ibánhez & Rocha, 2016).

Because bulk TOC measurements at low OC levels are disadvantageous in terms of analytic precision, we extracted and analyzed the resuspendable fine fraction of the sediments in the upper layer. The seasonal trend in the OC content of the fine fraction shows that more OC is available in the spring and summer months (Figure 5h), and OC remineralization rates, derived from O_2 consumption rates, are directly correlated to this seasonal increase (Figure 5i). This demonstrates that the resuspendable fine fraction is an important OC-pool, which regulates O_2 consumption rates in sandy sediments. The conversion of the sediment's fine OC content to bulk dry sediment mass (assuming a dry sediment density of 2 g/cm³) shows that this fraction accounts for between 0.0004 and 0.0007 wt. % of the sediment. Therefore, changes over the seasons are close to the precision of the TOC measurement of 0.0005 wt. % and cannot be resolved by analyzing the bulk sediment.

The seasonality of OC content in the fine fraction indicates the labile pool of OC that is readily consumed, whereas the rest of the bulk TOC appears to be refractory. The reaction rates at depth especially in winter are very low (2–3 µmol l^{-1} h^{-1}) despite sufficient O_2 supply, so that a complete mineralization of the bulk TOC would require more than 100 days. In contrast, assuming that only the resuspendable fine OC is used for respiration, this turnover time is significantly reduced. From the slope of the linear correlation between the content of fine OC and OC remineralization rates, a carbon specific degradation rate of 0.36 days^{-1} can be derived (Figure 5i). This means that 36% of fine OC is respired per day, and a complete degradation would take less than 3 days. The x-axis intercept of 3.7 mg l$_{Sed}$$^{-1}$ (Figure 5i) indicates the practically inert fine OC content. From the difference between the mean OC content in the fine fraction in August and the mean OC content in December and February (Figure 5i), we also calculated the excess in labile OC available in summer compared to OC at low reactivity in winter. The excess OC content is 4 mg C per l wet sediment. Applying the average O_2 consumption rate in August in the upper 15 cm (27 µmol l^{-1} h^{-1}, Figure 4e), it would take about 2 days to respire this excess OC. Taken together, these results confirm the rapid turnover of OC in intertidal beach sands and emphasize how the fast replenishment of labile OC controls the reaction rates, indicating a persistent carbon limitation. With regard to the influence of morphodynamics on the spatial distribution of reactive OC, this suggests that memory effects due to the burial of a previous upper layer only persist over a timescale of a few days.

The OC remineralization calculated from O_2 consumption rates (Figure 6) was integrated for the entire seawater infiltration zone and for a complete yearly cycle. As discussed in Section 4.1, the O_2 consumption characterizes this zone as a high throughput system. In terms of OC, 9.5 kg of C are being remineralized per m shoreline and year, which amounts to 110 t of C for the entire North Beach of Spiekeroog island with a length of about 11.5 km. In terms of CO_2, 35 kg are produced per m shoreline and year. Thus, the infiltration zone of the intertidal beach aquifer potentially acts as a strong source of CO_2, fueling the flux of dissolved inorganic C to the coastal ocean as previously reported (Charbonnier et al., 2022; Liu et al., 2021). The calculated C fluxes reflect microbial respiration in the upper beach meter and therefore represent a first estimate. The rates are assumed to be not O_2-limited and the observation of a fully oxic upper meter of the 40 m long infiltration zone proved this assumption to be reasonable except for small fractions in May and June (Table 1). It is expected that the oxic zone extends to greater depth, adding to the aerobic mineralization of organic carbon and thus to the budget we present for the upper meter. However, quantifying these rates and investigating the response of the seasonal OM input on the position of the oxycline remain a task for future studies.

5. Conclusion

We measured and analyzed the sedimentary O_2 consumption in the upper meter of an intertidal infiltration zone of a beach aquifer as a function of seasonal inputs of OM and O_2 through seawater infiltration, POM retention in the sand body, and morphodynamics. Our study reveals that O_2 consumption exhibits a strong seasonal depth dependency. In summer, we found rates up to 106 µmol l^{-1} h^{-1} in the first decimeters with an up to 40-fold decline with depth, whereas in winter, rates decreased significantly to less than 11 µmol l^{-1} h^{-1} throughout the upper meter. These dynamics indicate that O_2 consumption is fueled by the interplay of increasing OM loading in summer and reactive POM retention in the sand body, forming a reactive surface layer (Figure 7). Increasing rates during the warmer months lead to overall extensive O_2 consumption and a flux of up to 186 mmol O_2 per m^2 and day, corresponding to 69 g C per m shoreline and day, in the upper meter. The resulting OM remineralization characterizes the infiltration zone as a high-throughput system. Particularly in summer, OM is rapidly transformed in the retention layer, and observed seasonal changes in the OC content of the sand's suspendable particulate matter fraction indicate a high turnover of this OC pool within a few days and no long-term OC storage. From this, it can be concluded that the beach bioreactor is carbon-limited. Morphodynamics play a limited role in this process, as the reactive retention layer is occasionally buried by sediment deposition, leading to a short temporal occurrence of secondary rate peaks, but the system adapts to this change very quickly. In summary, this study highlights the significant role of fresh reactive OM availability in beach aquifers as a major contributor to subsurface microbial rates and associated biogeochemical turnover. The findings of this investigation can be used to constrain where and at what rate biogechemical processes occur in beach aquifers for future modeling approaches. They can also be used as a basis for extrapolation of OC remineralization during seawater infiltration and for a deeper understanding of nutrient cycling along the world's coastlines.

Data Availability Statement

The produced data used for O_2 consumption rates, sediment OC, O_2 distribution, grain size, and beach topography in the study are available at PANGAEA-Data Publisher for Earth & Environmental Science (Auer et al., 2024a, 2024b).

References

Ahmerkamp, S., Marchant, H. K., Peng, C., Probandt, D., Littmann, S., Kuypers, M. M. M., & Holtappels, M. (2020). The effect of sediment grain properties and porewater flow on microbial abundance and respiration in permeable sediments. *Scientific Reports*, *10*(1), 3573. https://doi.org/10.1038/s41598-020-60557-7

Ahmerkamp, S., Winter, C., Krämer, K., de Beer, D., Janssen, F., Friedrich, J., et al. (2017). Regulation of benthic oxygen fluxes in permeable sediments of the coastal ocean: Regulation of benthic oxygen fluxes. *Limnology & Oceanography*, *62*(5), 1935–1954. https://doi.org/10.1002/lno.10544

Ahrens, J., Beck, M., Marchant, H. K., Ahmerkamp, S., Schnetger, B., & Brumsack, H. (2020). Seasonality of organic matter degradation regulates nutrient and metal net fluxes in a high energy sandy beach. *Journal of Geophysical Research: Biogeosciences*, *125*(2), e2019JG005399. https://doi.org/10.1029/2019JG005399

Anschutz, P., Smith, T., Mouret, A., Deborde, J., Bujan, S., Poirier, D., & Lecroart, P. (2009). Tidal sands as biogeochemical reactors. *Estuarine, Coastal and Shelf Science*, *84*(1), 84–90. https://doi.org/10.1016/j.ecss.2009.06.015

Auer, F., Ahmerkamp, S., Cueto, J., Winter, C., & Holtappels, M. (2024a). Beach topography data of Spiekeroog island North Beach, May 2022 to April 2023 [Dataset]. PANGAEA. Retrieved from https://doi.pangaea.de/10.1594/PANGAEA.971356

Auer, F., Ahmerkamp, S., Cueto, J., Winter, C., & Holtappels, M. (2024b). Oxygen consumption rate, organic carbon and grain size data for intertidal sediments and oxygen concentration of pore waters data of Spiekeroog Island North Beach, May 2022 to April 2023 [Dataset]. PANGAEA. Retrieved from https://doi.pangaea.de/10.1594/PANGAEA.971357

Beck, M., Reckhardt, A., Amelsberg, J., Bartholomä, A., Brumsack, H.-J., Cypionka, H., et al. (2017). The drivers of biogeochemistry in beach ecosystems: A cross-shore transect from the dunes to the low-water line. *Marine Chemistry*, *190*, 35–50. https://doi.org/10.1016/j.marchem.2017.01.001

Boudreau, B. P., Huettel, M., Forster, S., Jahnke, R. A., McLachlan, A., Middelburg, J. J., et al. (2001). Permeable marine sediments: Overturning an old paradigm. *Eos, Transactions American Geophysical Union*, *82*(11), 133–136. https://doi.org/10.1029/EO082i011p00133-01

Calvo-Martin, E., Álvarez-Salgado, X. A., Rocha, C., & Ibánhez, J. S. P. (2021). Reactive Solute Transport Through Two Contrasting Subterranean Estuary Exit Sites in the Ría de Vigo (NW Iberian Peninsula). *Frontiers in Marine Science*, *8*, 626813. https://doi.org/10.3389/fmars.2021.626813

Charbonnier, C., Anschutz, P., Abril, G., Mucci, A., Deirmendjian, L., Poirier, D., et al. (2022). Carbon dynamics driven by seawater recirculation and groundwater discharge along a forest-dune-beach continuum of a high-energy meso-macro-tidal sandy coast. *Geochimica et Cosmochimica Acta*, *317*, 18–38. https://doi.org/10.1016/j.gca.2021.10.021

Charbonnier, C., Anschutz, P., Deflandre, B., Bujan, S., & Lecroart, P. (2016). Measuring pore water oxygen of a high-energy beach using buried probes. *Estuarine, Coastal and Shelf Science*, *179*, 66–78. https://doi.org/10.1016/j.ecss.2015.12.004

Charbonnier, C., Anschutz, P., Poirier, D., Bujan, S., & Lecroart, P. (2013). Aerobic respiration in a high-energy sandy beach. *Marine Chemistry*, *155*, 10–21. https://doi.org/10.1016/j.marchem.2013.05.003

Cogswell, C., & Heiss, J. W. (2021). Climate and seasonal temperature controls on biogeochemical transformations in unconfined coastal aquifers. *Journal of Geophysical Research: Biogeosciences*, *126*(12), e2021JG006605. https://doi.org/10.1029/2021JG006605

E.U. Copernicus Marine Service Information (CMEMS). (2023). Atlantic—European North West Shelf—Ocean biogeochemistry analysis and forecast. https://doi.org/10.48670/moi-00056

E.U. Copernicus Marine Service Information (CMEMS). (2024). Atlantic—European North West Shelf—Ocean Physics analysis and forecast. https://doi.org/10.48670/moi-00054

Garcia, H. E., & Gordon, L. I. (1992). Oxygen solubility in seawater: Better fitting equations. *Limnology & Oceanography*, *37*(6), 1307–1312. https://doi.org/10.4319/lo.1992.37.6.1307

Greskowiak, J., Seibert, S. L., Post, V. E. A., & Massmann, G. (2023). Redox-zoning in high-energy subterranean estuaries as a function of storm floods, temperatures, seasonal groundwater recharge and morphodynamics. *Estuarine, Coastal and Shelf Science*, *290*, 108418. https://doi.org/10.1016/j.ecss.2023.108418

Grünenbaum, N., Ahrens, J., Beck, M., Gilfedder, B. S., Greskowiak, J., Kossack, M., & Massmann, G. (2020). A multi-method approach for quantification of in- and exfiltration rates from the subterranean estuary of a high energy beach. *Frontiers in Earth Science*, *8*, 571310. https://doi.org/10.3389/feart.2020.571310

Grünenbaum, N., Greskowiak, J., Sültenfuß, J., & Massmann, G. (2020). Groundwater flow and residence times below a meso-tidal high-energy beach: A model-based analyses of salinity patterns and 3H-3He groundwater ages. *Journal of Hydrology*, *587*, 124948. https://doi.org/10.1016/j.jhydrol.2020.124948

Heiss, J. W., & Michael, H. A. (2014). Saltwater-freshwater mixing dynamics in a sandy beach aquifer over tidal, spring-neap, and seasonal cycles. *Water Resources Research*, *50*(8), 6747–6766. https://doi.org/10.1002/2014WR015574

Herrling, G., & Winter, C. (2014). Morphological and sedimentological response of a mixed-energy barrier island tidal inlet to storm and fair-weather conditions. *Earth Surface Dynamics*, *2*(1), 363–382. https://doi.org/10.5194/esurf-2-363-2014

Herrling, G., & Winter, C. (2015). Tidally- and wind-driven residual circulation at the multiple-inlet system East Frisian Wadden Sea. *Continental Shelf Research*, *106*, 45–59. https://doi.org/10.1016/j.csr.2015.06.001

Huettel, M., Berg, P., & Kostka, J. E. (2014). Benthic exchange and biogeochemical cycling in permeable sediments. *Annual Review of Marine Science*, *6*(1), 23–51. https://doi.org/10.1146/annurev-marine-051413-012706

Huettel, M., & Rusch, A. (2000). Transport and degradation of phytoplankton in permeable sediment. *Limnology & Oceanography*, *45*(3), 534–549. https://doi.org/10.4319/lo.2000.45.3.0534

Ibánhez, J. S. P., & Rocha, C. (2016). Oxygen transport and reactivity within a sandy seepage face in a mesotidal lagoon (Ria Formosa, Southwestern Iberia): Oxygen transport and reactivity. *Limnology & Oceanography*, *61*(1), 61–77. https://doi.org/10.1002/lno.10199

Kim, K. H., Heiss, J. W., Geng, X., & Michael, H. A. (2020). Modeling hydrologic controls on particulate organic carbon contributions to beach aquifer biogeochemical reactivity. *Water Resources Research*, *56*(10), e2020WR027306. https://doi.org/10.1029/2020WR027306

Kim, K. H., Heiss, J. W., Michael, H. A., Cai, W., Laattoe, T., Post, V. E. A., & Ullman, W. J. (2017). Spatial patterns of groundwater biogeochemical reactivity in an intertidal beach aquifer. *Journal of Geophysical Research: Biogeosciences*, *122*(10), 2548–2562. https://doi.org/10.1002/2017JG003943

Kim, K. H., Michael, H. A., Field, E. K., & Ullman, W. J. (2019). Hydrologic shifts create complex transient distributions of particulate organic carbon and biogeochemical responses in beach aquifers. *Journal of Geophysical Research: Biogeosciences*, *124*(10), 3024–3038. https://doi.org/10.1029/2019JG005114

Liu, Y., Jiao, J. J., Liang, W., Santos, I. R., Kuang, X., & Robinson, C. E. (2021). Inorganic carbon and alkalinity biogeochemistry and fluxes in an intertidal beach aquifer: Implications for ocean acidification. *Journal of Hydrology*, *595*, 126036. https://doi.org/10.1016/j.jhydrol.2021.126036

Luijendijk, A., Hagenaars, G., Ranasinghe, R., Baart, F., Donchyts, G., & Aarninkhof, S. (2018). The state of the world's beaches. *Scientific Reports*, *8*(1), 6641. https://doi.org/10.1038/s41598-018-24630-6

Massmann, G., Abarike, G., Amoako, K., Auer, F., Badewien, T. H., Berkenbrink, C., et al. (2023). The DynaDeep observatory – A unique approach to study high-energy subterranean estuaries. *Frontiers in Marine Science*, *10*, 1189281. https://doi.org/10.3389/fmars.2023.1189281

McLachlan, A., & Turner, I. (1994). The interstitial environment of sandy beaches. *Marine Ecology*, *15*(3–4), 177–212. https://doi.org/10.1111/j.1439-0485.1994.tb00053.x

Moore, W. S. (1999). The subterranean estuary: A reaction zone of ground water and sea water. *Marine Chemistry*, *65*(1–2), 111–125. https://doi.org/10.1016/S0304-4203(99)00014-6

Probandt, D., Eickhorst, T., Ellrott, A., Amann, R., & Knittel, K. (2018). Microbial life on a sand grain: From bulk sediment to single grains. *The ISME Journal*, *12*(2), 623–633. https://doi.org/10.1038/ismej.2017.197

Rao, A. M. F., McCarthy, M. J., Gardner, W. S., & Jahnke, R. A. (2007). Respiration and denitrification in permeable continental shelf deposits on the South Atlantic Bight: Rates of carbon and nitrogen cycling from sediment column experiments. *Continental Shelf Research*, *27*(13), 1801–1819. https://doi.org/10.1016/j.csr.2007.03.001

Reckhardt, A., Beck, M., Seidel, M., Riedel, T., Wehrmann, A., Bartholoma, A., et al. (2015). Carbon, nutrient and trace metal cycling in sandy sediments: A comparison of high-energy beaches and backbarrier tidal flats. *14*.

Reckhardt, A., Meyer, R., Seibert, S. L., Greskowiak, J., Roberts, M., Brick, S., et al. (2024). Spatial and temporal dynamics of groundwater biogeochemistry in the deep subsurface of a high-energy beach. *Marine Chemistry*, *264*.

Redfield, A. C., Ketchum, B. H., & Richards, F. A. (1963). The influence of organisms on the composition of sea-water. *The Sea: Ideas and Observations on Progress in the Study of the Seas*. Retrieved from https://www.vliz.be/en/imis?module=ref&refid=28944&printversion=1&dropIMIStitle=1

Robinson, C., Gibbes, B., & Li, L. (2006). Driving mechanisms for groundwater flow and salt transport in a subterranean estuary. *Geophysical Research Letters*, *33*(3), L03402. https://doi.org/10.1029/2005GL025247

Robinson, C., Li, L., & Barry, D. A. (2007). Effect of tidal forcing on a subterranean estuary. *Advances in Water Resources*, *30*(4), 851–865. https://doi.org/10.1016/j.advwatres.2006.07.006

Rocha, C. (2008). Sandy sediments as active biogeochemical reactors: Compound cycling in the fast lane. *Aquatic Microbial Ecology*, *53*, 119–127. https://doi.org/10.3354/ame01221

Seidel, M., Beck, M., Greskowiak, J., Riedel, T., Waska, H., Suryaputra, N. A., et al. (2015). Benthic-pelagic coupling of nutrients and dissolved organic matter composition in an intertidal sandy beach. *Marine Chemistry*, *176*, 150–163. https://doi.org/10.1016/j.marchem.2015.08.011

Spiteri, C., Slomp, C. P., Charette, M. A., Tuncay, K., & Meile, C. (2008). Flow and nutrient dynamics in a subterranean estuary (Waquoit Bay, MA, USA): Field data and reactive transport modeling. *Geochimica et Cosmochimica Acta*, *72*(14), 3398–3412. https://doi.org/10.1016/j.gca.2008.04.027

Waska, H., Greskowiak, J., Ahrens, J., Beck, M., Ahmerkamp, S., Böning, P., et al. (2019). Spatial and temporal patterns of pore water chemistry in the inter-tidal zone of a high energy beach. *Frontiers in Marine Science*, *6*, 154. https://doi.org/10.3389/fmars.2019.00154

Wilson, S. J., Moody, A., McKenzie, T., Cardenas, M. B., Luijendijk, E., Sawyer, A. H., et al. (2024). Global subterranean estuaries modify groundwater nutrient loading to the ocean. *Limnology and Oceanography Letters, lol2, 9*(4), 10390–10422. https://doi.org/10.1002/lol2.10390

Wright, L. D., & Short, A. D. (1984). Morphodynamic variability of surf zones and beaches: A synthesis. *Marine Geology, 56*(1–4), 93–118. https://doi.org/10.1016/0025-3227(84)90008-2

Zhou, Z., Henkel, S., Kasten, S., & Holtappels, M. (2023). The iron "redox battery" in sandy sediments: Its impact on organic matter remineralization and phosphorus cycling. *Science of The Total Environment, 865*, 161168. https://doi.org/10.1016/j.scitotenv.2022.161168

Zhou, Z., Waska, H., Henkel, S., Dittmar, T., Kasten, S., & Holtappels, M. (2024). Iron promotes the retention of terrigenous dissolved organic matter in subtidal permeable sediments. *Environmental Science & Technology, 58*(14), 6204–6214. https://doi.org/10.1021/acs.est.3c09531